Available online at www.sciencedirect.com
SCIENCE DIRECT®
Chemical Physics Letters 374 (2003) 110–118
CHEMICAL PHYSICS LETTERS
www.elsevier.com/locate/cplett

Fluorescence lifetime and nonradiative relaxation dynamics of DCM in nonpolar solvent

Chih-Wei Chang, Ya-Ting Kao, Eric Wei-Guang Diau *

Department of Applied Chemistry and Center for Interdisciplinary Molecular Science, National Chiao Tung University, Hsinchu 30050, Taiwan, ROC

Received 17 March 2003; in final form 8 April 2003

Abstract

The nonradiative dynamics of DCM in hexane have been investigated using femtosecond fluorescence up-conversion technique at three excitation wavelengths (400, 445 and 480 nm). The S_1 lifetime was observed to be 9.8 ± 0.5 ps, which is independent of the excitation and the fluorescence wavelengths. The observed S_1 lifetimes of DCJT and DCJTB are slower than those of DCM and DCMB by one order of magnitude, indicating the significance of the twisting motion of the amino group affecting the S_1 nonradiative dynamics. TDDFT calculations suggest that an intersystem crossing is responsible for the observed S_1 dynamics of DCM in nonpolar solvent.
© 2003 Elsevier Science B.V. All rights reserved.

1. Introduction

The 4-(dicyanomethylene)-2-methyl-6-*p*-(dimethylamino)styryl-4H-pyran (DCM) molecule is well-known as a very efficient laser dye which is widely used for a tunable light source in a broad spectral region [1,2]. Recent commercial advances in the development of full color graphical displays [3,4] have made DCM and its derivatives as potential candidates for red dopant materials in the applications of organic light emitting diode (OLED) devices [5–8]. Therefore, the DCM molecule has attracted much attention in the characterization of the excited-state properties in bulk solutions [9–20] and biological environments [21]. Moreover, the molecule has been selected as a target molecule for the spectral phases controlling experiments [22].

The steady-state absorption and fluorescence spectra of DCM [10,12,20] show that the molecule exhibits large Stokes shifts in polar solvents depending on the polarity of the solvents [23]; the change of the dipole moment upon excitation is dramatic [11,12]. The large dipole moment of the fluorescent state is a typical feature for the molecule to involve an emissive charge transfer (CT) state. The lifetime of the fluorescent state of DCM is on the order of nanoseconds [9–11] while the solvent relaxation occurs on the sub-picosecond to the picosecond time scale [14–19]; both depending on the solvent polarity.

* Corresponding author.
E-mail address: diau@mail.ac.nctu.edu.tw (E.W.-G. Diau).
URL: http://diau08.ac.nctu.edu.tw.

0009-2614/03/$ - see front matter © 2003 Elsevier Science B.V. All rights reserved.
doi:10.1016/S0009-2614(03)00645-6

The structure of DCM is characterized by the arylidene moiety with a dimethylamino electron donor group linked to two cyano electron acceptor groups by a conjugated bridge (Scheme 1). Photoexcitation of DCM to its first absorption band put the excited molecule in the locally excited (LE) state (S_1) and two conformational changes may thus result: Rotation about the central CC double bond leads to the *trans* → *cis* isomerization via a phantom singlet state which is a typical photochemical process occurring on *trans*-stilbene [24] and many olefin molecules [25]; twisting of the dimethylamino group gives a highly polar twisted intramolecular charge transfer (TICT) state which can be stabilized by polar solvents as being discussed in the system of 4-dimethyl-aminobenzonitrile (DMABN) [25,26]. For DCM, the mechanism of the transition from the LE state to the CT (or TICT) state is still unclear but the theoretical calculations [13] have indicated the following dynamical picture. First, a small energy barrier (~0.2 eV) was predicted on the potential energy surface (PES) of the S_1-LE state along the pathway of twisting of the central CC double bond, and the barrier height is insensitive to the change of the solvent polarity. Second, along the pathway of twisting the CN single bond of the dimethylamino group of DCM in solvent, the shape of the excited-state PESs is strongly affected by the polarity of the solvent and the choice of the solvation model [13]. In a polar solution, the energy of the S_1-LE state increases whereas the energy of the S_2-CT state decreases by twisting the CN single bond of the dimethylamino group, and this would lead to a nonadiabatic curve crossing between the two states. Therefore, with increasing the polarity of the solvent, the formation of an emissive TICT state along the amino twisting coordinate is the result of the theoretical prediction. Third, in polar solvents when the TICT state is formed at the perpendicular geometry where the energy of the S_1-LE state is higher than that of the S_2-CT state, the energy barrier in the TICT state along the torsional coordinate of the CC double bond would increase substantially and this may prevent the *trans* → *cis* isomerization to occur in polar solvents.

Early experimental results show that the *trans* to *cis* photoisomerization yield of DCM increases dramatically in nonpolar solvents [10,12]. Since the energy barrier of DCM in the S_1-LE state along the *trans* → *cis* isomerization coordinate was cal-

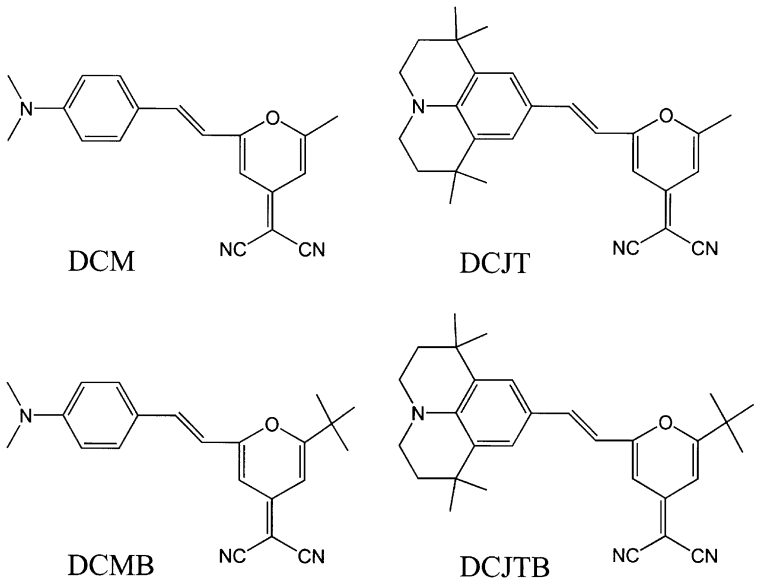

Scheme 1.

culated to be unaffected by the solvent polarity, the experimental evidence implies that there may exist another relaxation channel resulting in the formation of substantial amounts of the *cis* product observed in nonpolar solvents. To unravel the issue for what the relaxation channel could be, we have investigated the nonradiative relaxation dynamics of DCM in hexane using femtosecond (fs) fluorescence up-conversion technique. To further demonstrate the dynamical effect of the conformational change via twisting the dimethylamino group of the dye molecule, the *tert*-butyl substituted DCM derivative (DCMB; Scheme 1) and two julolidyl DCM derivatives (DCJT and DCJTB; Scheme 1) were also studied for comparison. Theoretical calculations were performed using the time-dependent density functional theory (TDDFT) method for the excited-state surface scan of DCM along the CCNC torsional coordinate of the amino group.

2. Experimental

The time-resolved fluorescence measurements were carried out using an integrated fluorescence optically gated system (FOG100, CDP) in combination with a mode-locked Ti:sapphire laser (Mira 900D, Coherent) pumped by a 10 W Nd:YVO_4 laser (Verdi-V10, Coherent). The details of the experimental setup have been described elsewhere [27]. Briefly, the femtosecond laser system generates a 76 MHz pulse train in a tunable range of 700–1000 nm. The output of the pulse was tuned to the center wavelengths of 800, 890 and 960 nm with the average power being 1.6, 1.2 and 0.6 W, respectively. Typically the FWHM of the spectral profile of the pulse is in the range of 10–12 nm and the FWHM of the autocorrelation is in the range of 140–160 fs. The fs pulses were frequency-doubled to provide appropriate excitation wavelengths ($\lambda_{ex} = 400$, 445 and 480 nm). A dichroic beam splitter was used to separate the frequency-doubled pulses (as pump/excitation) and the fundamental pulses (as probe/gate). The excitation pulses were appropriately attenuated and then focused onto a 1-mm thick rotating cell containing the sample solution. The fluorescence emitted from the sample at ambient temperature (24 ± 0.5 °C) was collected by a lens pair and focused on a 0.5-mm thick BBO type-I crystal. The gate pulses passed a stepping motor-driven translational stage (maximum delay time is 2.0 ns and minimum step length is 6.25 fs) and were also focused on this crystal for sum-frequency generation (SFG). The fluorescence wavelength ($\lambda_f = 500$–620 nm) to be up-converted by SFG was selected by changing the phase-matching angle of the BBO crystal. The up-converted signal was spatially and spectrally separated from the other interfering lights by a combination of an iris, a band-pass filter, and a monochromator (CDP2022, reciprocal dispersion is 8.7 nm/mm) and then detected by a photomultiplier tube (R1527P, Hamamatsu) connected to a computer-controlled photon-counting system. For each λ_f, the transient profile was obtained by varying the delay time between the pump pulse and the gate pulse through the optical delay line. In order to avoid the reorientation effects of the dye molecule, the polarization between the pump and the gate pulses was fixed at the magic angle configuration throughout all the measurements.

The UV–visible absorption spectra were recorded with a double array spectrophotometer

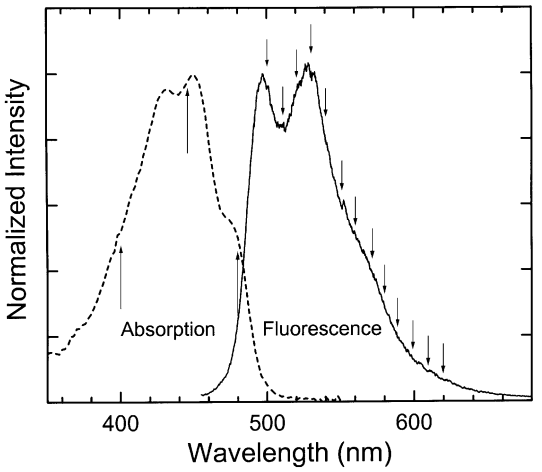

Fig. 1. Steady-state absorption (dotted curve) and fluorescence (solid curve; $\lambda_{ex} = 445$ nm) spectra of DCM in hexane. The upward arrows in the absorption spectrum represent the locations of the excitation wavelengths and the downward arrows in the fluorescence spectrum indicate the wavelengths to be up-converted in the time-resolved experiments.

(HP 8452A) and the fluorescence spectra were obtained with a spectrophotofluorometer (Hitachi F-4500). The steady-state absorption and emission ($\lambda_{ex} = 445$ nm) spectra of the DCM/hexane solution are shown in Fig. 1.

DCM was purchased from Exciton and used without further purification. DCMB, DCJT, and DCJTB are synthesized according to the procedures patented by Eastman Kodak Company [28,29]. Because the solubility of the dye molecules in hexane (Merck UVASOL) is quite low [20] which leads to the problem of aggregation evidenced by the emission spectra, a saturated solution was first prepared and then passed through a particle filter to remove the aggregated particles in the solution. All solutions were freshly prepared in a dim room and kept in the dark prior to the experiment.

3. Results and data analysis

The experimental data were analyzed according to an appropriate kinetic model with convolution of the laser pulses. The influence of the group velocity dispersion (GVD) must be considered because different spectral components will propagate with different speed through the sample cell and the optics used to collect the emission. As a result, the location of time zero and the FWHM of the instrumental response function (IRF) are varied as a function of the wavelength of the up-converted signal [27]. Therefore, the zero of the pump/gate delay time, the FWHM of the IRF, and the decay time constant of the kinetics were determined as floating parameters in the fitting procedure. The typical transient profiles observed at $\lambda_f = 560$ nm with the excitation wavelengths $\lambda_{ex} = 400$, 445 and 480 nm are shown in Figs. 2a–c, respectively. The transients are well characterized by a single exponential function with the decay time constants of 9.9, 9.7 and 10.1 ps at $\lambda_{ex} = 400$, 445 and 480 nm, respectively. Since the measured time constants are independent of both excitation and fluorescence (see below) wavelengths within the experimental uncertainty, we thus made an average for the values obtained from total 39 independent measurements at various λ_{ex} and λ_f. This gives a value

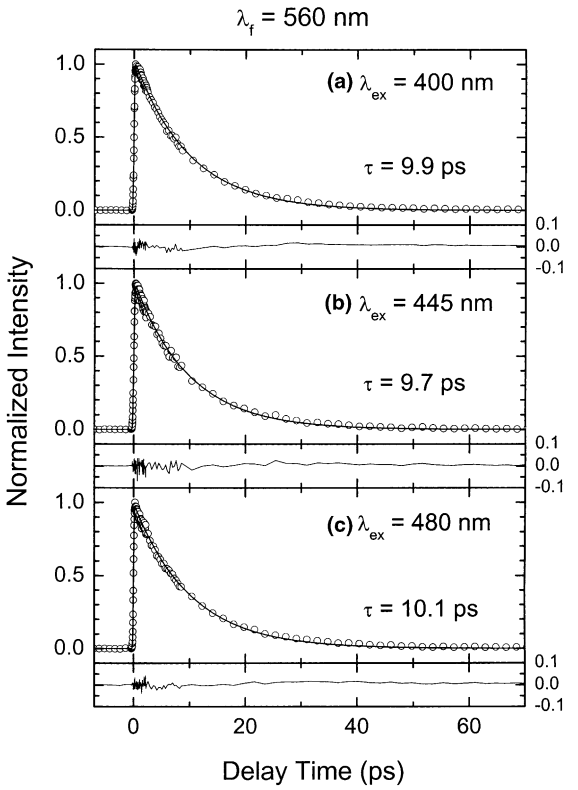

Fig. 2. Time-resolved fluorescence up-converted signals of DCM in hexane obtained at $\lambda_f = 560$ nm with various excitation wavelengths: (a) $\lambda_{ex} = 400$ nm; (b) $\lambda_{ex} = 445$ nm; (c) $\lambda_{ex} = 480$ nm. The data are shown as symbols and the fitted results indicated as solid curves with the corresponding residuals of each fit shown in the lower panels. The kinetics of the transients are modeled by a single exponential decay function with convolution of laser pulses; the fitted time constants are indicated.

of 9.8 ± 0.5 ps to be reported for the observed S_1 lifetime of DCM in hexane; where the reported uncertainty represents two standard statistical errors.

The time-resolved fluorescence spectra of DCM were constructed with the relative intensity of each transient in the spectral range of 500–620 nm being adjusted according to the normalized intensity of the steady-state spectrum (Fig. 1) with 10 nm intervals. The reconstruction procedure is based on the method developed by Maroncelli and Fleming [30] and it is summarized as follows. First, the transient obtained at a given wavelength λ_f is fitted to a theoretical curve with proper kinetics ac-

cording to the above-mentioned procedure. Second, the theoretical curve is integrated by time and the value from integration is adjusted with a scaling factor to match the normalized intensity of the steady-state fluorescence spectrum at the wavelength λ_f. Third, the 'matched' scaling factor is used to scale the intensity of the theoretical transient at the wavelength λ_f. Finally, repeat the above steps for the other transients taken at different wavelengths and sort the scaled theoretical transients with the increasing order of wavelengths, a three-dimensional fluorescence profile can be constructed (Fig. 3a). The specific time-resolved fluorescence spectrum can be obtained from cutting the 3-D profile parallel to the axis direction of λ_f and converting the wavelengths to the wavenumbers at each delay time; the results are shown in Fig. 3b for the delay times ranging from 0.3 to 30 ps. The intensities of the time-resolved emission spectra were integrated by wavenumber at selected delay times to provide the overall kinetics of the spectral profiles. The integral values as a function of delay time are shown in Fig. 3c with the kinetics modeled by a single exponential decay time constant of 9.6 ps.

From the structural viewpoint, the dynamical effect of the twisting motion of the dimethylamino group in DCM is an interesting subject to study. For this reason we have investigated the other two julolidyl DCM derivatives (DCJT and DCJTB) with the excitation at $\lambda_{ex} = 445$ nm. The transients of DCJT and DCJTB observed at $\lambda_f = 560$ nm are shown in Fig. 4 to compare with those of DCM and DCMB. The julolidyl DCM dyes show apparently longer lifetimes than their unlocked counterparts and the corresponding kinetics can be described by a single exponential decay function with the time constants of 77.5 and 70.0 ps for DCJT (Fig. 4a) and DCJTB (Fig. 4b), respectively.

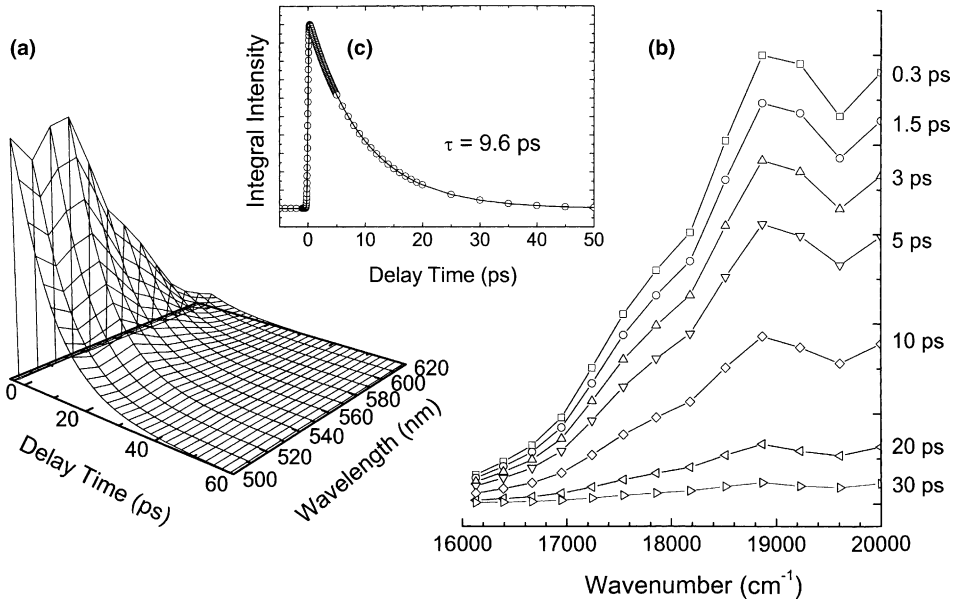

Fig. 3. (a) A three-dimensional view of the fitted transients of DCM in hexane based on the raw data obtained at $\lambda_{ex} = 445$ nm (see text for details) showing the normalized temporal profiles in the spectral range of 500–620 nm with 10 nm intervals. (b) The time-resolved fluorescence spectra of DCM obtained from cutting the 3D surface of (a) along the direction parallel to the wavelength axis at each specified delay time. (c) The wavenumber-integrated intensity as a function of delay time showing the global kinetics of the time-resolved fluorescence spectra in (a). The circles represent the integral values at the selected delay times and the solid curve is the fitted result characterized by a single exponential decay function with $\tau = 9.6$ ps.

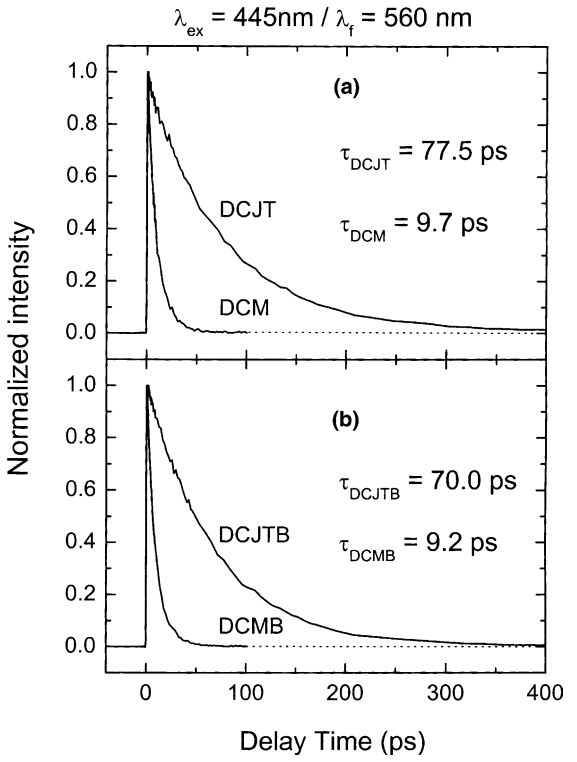

Fig. 4. Time-resolved fluorescence up-converted signals of (a) DCM vs. DCJT and (b) DCMB vs. DCJTB in hexane obtained at $\lambda_{ex} = 445$ nm and $\lambda_f = 560$ nm. The transients can be described by a single exponential function with the decay time constants as indicated.

4. Theoretical calculations

The geometries of DCM and DCJT on the ground state PES were fully optimized at the B3LYP/6-31G(d) level of theory. In order to confirm the optimized structure is a true minimum, vibrational frequencies were calculated at the same level of theory when the geometry optimization is successful. For DCM, a relaxed PES scan was further performed along the CCNC torsional coordinate (ϕ) at the B3LYP/6-31G(d) level with the step size of 10° in each calculation. At each point of the optimized potential energy curve along the CCNC torsional coordinate, the single-point excited-state calculations were carried out at the TD-B3LYP/6-31+G(d) levels of theory.

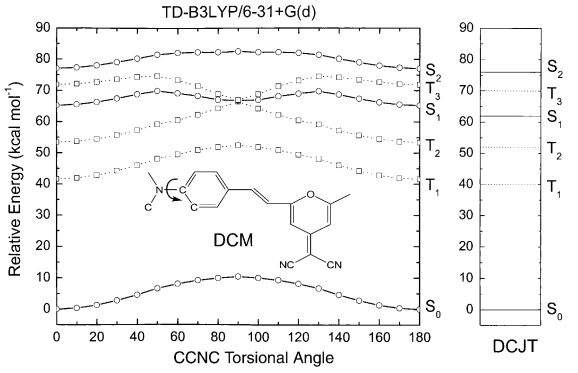

Fig. 5. Potential energy curves of isolated DCM along the CCNC torsional angle coordinate (ϕ) calculated at the TD-B3LYP/6-31+G(d) level of theory. The vertical excitation energies of DCJT at the FC geometry are shown in the right panel for comparison.

The calculated results for the ground state (S_0) and two low-lying singlet states (S_1 and S_2) as well as three low-lying triplet states (T_1, T_2 and T_3) are shown in Fig. 5. At the Franck–Condon (FC) structure, DCM belongs to C_s symmetry with all the heavy atoms located in the molecular symmetry plane. The S_1 state corresponds to a $\pi \rightarrow \pi^*$ transition with the vertical excitation energy calculated to be 65 kcal mol^{-1} above the S_0 state. Note that the position of the maximum intensity in the first absorption band of DCM in hexane occurs near $\lambda \sim 445$ nm (Fig. 1), which corresponds to an excitation energy of 64 kcal mol^{-1}. Therefore, the calculated vertical energy of the S_1 state agrees with the experimental result very well, provided the influence of the solvent is negligible. [1] The good agreement between theory and experiment indicates the reliability of the surface scan calculations along the ϕ coordinate and the significance of the calculated results will be discussed in the following section. All of the electronic structure calculations were performed using the Gaussian software package [31].

[1] Based on the reaction-field model using the formula provided by [13], the solvation energies of the S_0 and the S_1 states in hexane at the FC geometry are estimated to be −0.5 and −1.0 kcal mol^{-1}, respectively, the relevant parameters are the following: $\mu(S_0) = 8.4$ D, $\mu(S_1) = 12.4$ D, $a = 8$ Å, $n = 1.3749$, and $\varepsilon = 1.92$.

5. Discussion

The absorption and the steady-state emission spectra of DCM in hexane (Fig. 1; see also [20]) are characterized by the broad bands with vibrational structures forming mirror image to each other. According to the conclusion of an early study [32], the well-structured feature and the mirror similarity of both spectra of DCM in nonploar solvent are the indication of a planar nuclear geometry in both ground and excited states. Recent study has further simulated the evolution of the spectral band shapes of DCM in nonpolar and polar solvents by a two-state electronic model including the effects of solvent polarity and vibronic coupling [20]. In this study, we provide time-resolved information of DCM in hexane at various fluorescence wavelengths (Fig. 3) with three different excitations (Fig. 2) to gain insights for the understanding of the dynamical behavior of DCM on the excited-state PES. The results will be discussed in the following.

The scan of the time-resolved emission spectra was carried out at $\lambda_{ex} = 445$ nm with 13 temporal profiles obtained in the fluorescence wavelength region of 500–620 nm. The transients at each λ_f are well characterized by a single exponential function with the fitted decay time constants in the range of 9.3–10.4 ps and the results show no correlation with λ_f. This wavelength-independent feature of the S_1 lifetime is further visualized from the corresponding time-resolved emission spectra shown in Fig. 3: All the fluorescence spectra are similar in shape at any given delay time (Fig. 3b) and the overall spectral profile decays exponentially by a time constant of 9.6 ps (Fig. 3c). The observed negligible spectral shift is similar to the observation of Gustavsson et al. [16] that the mean frequency of the DCM fluorescence spectrum does not vary with time in chloroform. This phenomenon implies the insignificant solvation dynamic effect of DCM in nonpolar solvent and the observed simple excited-state dynamics of DCM may be inferred due only to a pure relaxation process free from the influence of the solvents.

In solutions, solvent molecules surely play a key role for the vibrational relaxation process to carry away the excess internal energy from the electronically energetic solute molecule. To examine the dynamical effect of the excess energy of DCM in the S_1-LE state, the fluorescence lifetime at two other excitation wavelengths, 400 and 480 nm, were measured. The transient profiles observed at $\lambda_f = 560$ nm with the excitation wavelengths $\lambda_{ex} = 400$, 445 and 480 nm are well characterized by a single exponential decay function with the time constants of 9.9, 9.7, and 10.1 ps, respectively (Fig. 2). Since the observed S_1 lifetime of DCM is independent of the excitation energy, the solvent-induced vibrational relaxation in the S_1-LE state is complete prior to the electronic relaxation and the observed fluorescence occurs from the vibrationally cold S_1-LE state. We found no evidence for the solvent-induced vibrational relaxation in the present study, but its time scale should be much shorter than the observed 10 ps, the overall depopulation time of DCM in the S_1-LE state.

We are now in the stage to find out a mechanism responsible for the observed 10 ps relaxation process of DCM in hexane. The electronically excited DCM is known to undergo *trans* → *cis* isomerization with the conversion yield particularly high in nonpolar solvents [10,12]. Because the *trans* → *cis* isomerization on the S_1 PES requires to overcome an energy barrier of ~0.2 eV [13], the lifetime measured near its 0–0 band origin ($\lambda_{ex} = 480$ nm) is the same as what measured with more than 0.5 eV excess internal energy ($\lambda_{ex} = 400$ nm) has ruled out the possibility for the isomerization process to occur directly from the S_1 state. Since the observed excited-state dynamics of DCM is not related to rotation of the central CC bond in the S_1 state, the dynamical effect of twisting the dimethylamino group of the molecule is the issue to be verified. For this purpose, we have investigated the excited-state dynamics of julolidyl DCM derivative (DCJT; Scheme 1) under the same condition as DCM. With the structural constraint for the motion of twisting of the dimethylamino group, the S_1 lifetime of DCJT was found to slow down drastically in comparison with that of DCM (Fig. 4a). To double confirm such a dramatic dynamical effect, another structural pair (DCMB and DCJTB) was chosen to study under the same experimental conditions. The S_1 lifetimes of DCMB

and DCJTB were measured to be 9.2 ps and 70.0 ps (Fig. 4b), respectively. Our results shown in Fig. 4 indicate that the relaxation time of DCM in the S_1 state has only slightly shortened upon *tert*-butyl substitution whereas the relaxation time has significantly lengthened by one order of magnitude when the twisting motion of the amino group is strictly prohibited. Therefore, the corresponding excited-state dynamics of DCM must be related to the twisting motion of the dimethylamino group.

To understand what happened to the variation of the excited-state PESs for twisting the amino group of DCM, we have carried out TDDFT calculations for the molecule to twist along the CCNC torsional angle coordinate (Fig. 5). Twisting of the CCNC torsional angle leads to the energy of the S_1 state to gradually increase and a saddle point may occur at $\phi = 50°$ or 130° with an energy barrier of $\sim$0.2 eV. Further following the twisting pathway, the S_1 potential energy curve starts to approach the T_2 and the T_3 curves and eventually the three curves would cross at the perpendicular conformation with $\phi = 90°$. Because the surface touching occurs between the S_1 and the T_2 states at $\phi = 90°$, the observed 9–10 ps S_1 lifetime in DCM and DCMB is considered to be due to an efficient $S_1 \rightarrow T_2$ intersystem crossing (ISC) process occurring at their twisting geometry. In the case of DCJT and DCJTB, on the other hand, the energy gap between the S_1 and the T_2 states cannot be substantially reduced since the amino group is bound and the twisting motion is restricted. Therefore, the $S_1 \rightarrow T_2$ ISC processes in DCJT and DCJTB are expected to be less efficient which could result in much longer S_1 lifetimes being observed ($\tau_{DCJT} = 77.5$ ps and $\tau_{DCJTB} = 70.0$ ps).

According to both the experimental and theoretical findings discussed above, a general mechanism is given below. First, upon excitation to the S_1-LE state, the observed excited-state dynamics of DCM in hexane is due to the $S_1 \rightarrow T_2$ ISC process involving the twisting motion of the dimethylamino group on the S_1 PES. Second, the $T_2 \rightarrow T_1$ internal conversion is expected to be a very efficient process to follow and the molecule would have sufficient internal energy to overcome a small energy barrier along the CC double bond rotation path on the relatively flat T_1 surface. [2] Third, both *trans* and *cis* isomers on the S_0 PES could result from rotating the CC double bond since the $T_1 \rightarrow S_0$ ISC process occurs most efficiently at the perpendicularly twisted CC double bond conformation where the two surfaces cross [13]. This mechanism may explain for the relatively high quantum yield of the *trans* $\rightarrow$ *cis* photoisomerization of DCM in nonpolar solvents [10,12]. Finally, in polar solutions, the significant dipole–dipole interaction must be taken into account. The energy of the S_2 state of DCM would be lowered significantly at the perpendicularly twisted conformation ($\phi = 90°$) where a TICT state could be formed with a large dipole moment being expected [13]. When the TICT state is lower in energy than all the other triplet states, the solvent-induced vibrational relaxation may play an important role so that the dominating ISC process in the nonpolar solution observed in this study could not happen if the dye molecule is dissolved in polar solvents. [3] In addition to the solvation dynamics of DCM in many polar solvents that have been studied in recent years [14–19], the electronic transition (relaxation) from the S_1-LE state to the S_2-CT state could be an important process to be considered to rationalize the complex excited-state dynamics of DCM in polar solvents. Work is currently in progress to provide a clear dynamic picture for understanding of the excited-state dynamics of DCM and its derivatives in polar solvents.

Acknowledgements

This work was supported by the National Science Council of Republic of China with the Project Contract Number NSC 91-2113-M-009-008. We sincerely acknowledge Prof. Chin H. Chen, a faculty member of Applied Chemistry Department and Microelectronics and Information System Research Center of NCTU, for many helpful discussions; the compounds of DCMB, DCJT and

[2] Refer to Fig. 5 in [13].

[3] For DCM dissolved in methanol, the $S_1 \rightarrow T_1$ ISC process was found to be insignificant with the quantum yield estimated to be less than 3×10^{-3} [12].

DCJTB were a very generous gift provided by Prof. Chen. The initial phase of the work by Mr. Cheng-Ii Lu is also acknowledged.

References

[1] P.R. Hammond, Opt. Commun. 29 (1979) 331.
[2] E.G. Marason, Opt. Commun. 37 (1981) 56.
[3] C.W. Tang, S.A. VanSlyke, Appl. Phys. Lett. 51 (1987) 913.
[4] L.S. Hung, C.H. Chen, Mater. Sci. Eng. R 39 (2002) 143.
[5] C.H. Chen, J. Shi, C.W. Tang, Macromol. Symp. 125 (1997) 1.
[6] Z.Y. Xie, L.S. Hung, S.T. Lee, Appl. Phys. Lett. 79 (2001) 1048.
[7] X.H. Zhang, B.J. Chen, X.Q. Lin, O.Y. Wong, C.S. Lee, H.L. Kwong, S.T. Lee, S.K. Wu, Chem. Mater. 13 (2001) 1565.
[8] B.-J. Jun, C.-B. Yoon, H.-K. Shim, L.-M. Do, T. Zyung, Adv. Funct. Mater. 11 (2001) 430.
[9] H.-K. Zhang, R.-L. Ma, E.-P. Niu, C. Guo, J. Photochem. 29 (1985) 397.
[10] J.M. Drake, M.L. Lesiecki, D.M. Camaioni, Chem. Phys. Lett. 113 (1985) 530.
[11] M. Meyer, J.C. Mialocq, M. Rougee, Chem. Phys. Lett. 150 (1988) 484.
[12] M. Meyer, J.-C. Mialocq, B. Perly, J. Phys. Chem. 94 (1990) 98.
[13] S. Marguet, J.C. Mialocq, P. Millie, G. Berthier, F. Momicchioli, Chem. Phys. 160 (1992) 265.
[14] D.C. Easter, A.P. Baronavski, Chem. Phys. Lett. 201 (1993) 153.
[15] H. Zhang, A.M. Jonkman, P. van der Meulen, M. Glasbeek, Chem. Phys. Lett. 224 (1994) 551.
[16] T. Gustavsson, G. Baldacchino, J.-C. Mialocq, S. Pommeret, Chem. Phys. Lett. 236 (1995) 587.
[17] M.M. Martin, P. Plaza, Y.H. Meyer, Chem. Phys. 192 (1995) 367.
[18] P. van der Meulen, H. Zhang, A.M. Jonkman, M. Glasbeek, J. Phys. Chem. 100 (1996) 5367.
[19] S.A. Kovalenko, N.P. Ernsting, J. Ruthmann, Chem. Phys. Lett. 258 (1996) 445.
[20] B. Boldrini, E. Cavalli, A. Painelli, F. Terenziani, J. Phys. Chem. A 106 (2002) 6286.
[21] D. Mandal, S. Sen, K. Bhattacharyya, T. Tahara, Chem. Phys. Lett. 359 (2002) 77, and references therein.
[22] S.-H. Lee, K.-H. Jung, J.H. Sung, K.-H. Hong, C.H. Nam, J. Chem. Phys. 107 (2002) 9858.
[23] J.R. Lakowicz, Principles of Fluorescence Spectroscopy, second ed., Kluwer Academic/Plenum Publishers, New York, 1999.
[24] J.S. Baskin, L. Banares, S. Pedersen, A.H. Zewail, J. Phys. Chem. 100 (1996) 11920.
[25] M. Klessinger, J. Michl, Excited States and Photochemistry of Organic Molecules, VCH Publishers, New York, 1995.
[26] Z.R. Grabowski, J. Dobkowski, Pure Appl. Chem. 55 (1983) 245.
[27] Y.-C. Lu, C.-W. Chang, E.W.-G. Diau, J. Chin. Chem. Soc. 49 (2002) 693.
[28] C.H. Chen, K.P. Klubek, J. Shi, US Patent 5908581, 1999.
[29] C.H. Chen, C.W. Tang, J. Shi, K.P. Klubek, Macromol. Symp. 125 (1997) 49.
[30] M. Maroncelli, G.R. Fleming, J. Chem. Phys. 86 (1987) 6221.
[31] M.J. Frisch et al., GAUSSIAN 98, Revision A.11, Gaussian Inc., Pittsburgh, PA, 1998.
[32] I.B. Berlman, J. Phys. Chem. 74 (1970) 3085.